

# A quantitative assessment of changes in seasonal potential predictability for the twentieth century

M. Azhar Ehsan · In-Sik Kang · Mansour Almazroui ·  
M. Adnan Abid · Fred Kucharski

Received: 25 July 2012 / Accepted: 8 July 2013 / Published online: 4 August 2013  
© Springer-Verlag Berlin Heidelberg 2013

**Abstract** Changes over the twentieth century in seasonal mean potential predictability (PP) of global precipitation, 200 hPa height and land surface temperature are examined by using 100-member ensemble. The ensemble simulations have been conducted by using an intermediate complexity atmospheric general circulation model of the International Center for Theoretical Physics, Italy. Using the Hadley Centre sea surface temperature (SST) dataset on a  $1^\circ$  grid, two 31 year periods of 1920–1950 and 1970–2000 are separated to distinguish the periods of low and high SST variability, respectively. The standard deviation values averaged for the (“Niño-3.4”;  $5^\circ\text{S}$ – $5^\circ\text{N}$ ,  $170^\circ\text{W}$ – $120^\circ\text{W}$ ) region are 0.71 and  $1.15^\circ\text{C}$ , for the periods of low and high SST variability, respectively, with a percentage change of 62 % during December–January–February (DJF). The leading eigenvector and the associated principal component time series, also indicate that the amplitude of SST variations have positive trend since 1920s to recent years, particularly over the El Niño Southern Oscillation (ENSO) region. Our hypothesis states that the increase in SST variability has increased the PP for precipitation, 200 hPa height and land surface temperature during the DJF. The

analysis of signal and noise shows that the signal-to-noise (S/N) ratio is much increased over most of the globe, particularly over the tropics and subtropics for DJF precipitation. This occurs because of a larger increase in the signal and at the same time a reduction in the noise, over most of the tropical areas. For 200 hPa height, the S/N ratio over the Pacific North American (PNA) region is increasing more than that for the other extratropical regions, because of a larger percentage increase in the signal and only a small increase in noise. It is also found that the increase in seasonal mean transient signal over the PNA region is 50 %, while increase in the noise is only 12 %, during the high SST variability period, which indicates that the increase in signal is more than the noise. For DJF land surface temperature, the perfect model notion is utilized to confirm the changes in PP during the low and high SST variability periods. The correlation between the perfect model and the other members clearly reveal that the seasonal mean PP changed. In particular, the PP for the 31 years period of 1970–2000 is higher than that for the 31 years period of 1920–1950. The land surface temperature PP is increased in northern and southern Africa, central Europe, southern South America, eastern United States and over Canada. The increase of the signal and hence the seasonal mean PP is coincides with an increase in tropical Pacific SST variability, particularly in the ENSO region.

---

M. A. Ehsan · I.-S. Kang · M. Almazroui (✉) · M. A. Abid  
Center of Excellence for Climate Change Research/Department  
of Meteorology, King Abdulaziz University,  
Jeddah 21589, Saudi Arabia  
e-mail: mansour@kau.edu.sa

I.-S. Kang  
School of Earth and Environmental Sciences,  
Seoul National University, Seoul, Korea

F. Kucharski  
International Center for Theoretical Physics, Trieste, Italy

**Keywords** Potential predictability · ENSO · Ensemble · Signal · Noise

## 1 Introduction

The central theme throughout this study is that the amplitude of sea surface temperature (SST) variability in the

tropical Pacific has increased during the twentieth century, and that the increase in SST variability, particularly in the El Niño–Southern Oscillation (ENSO) region, has increased the seasonal mean potential predictability of the atmospheric variables. The potential predictability, defined as the predictability of the model prescribed with perfect boundary (e.g. observed SST) conditions (Shukla et al. 2000; Kang and Shukla 2006). In present study, the potential predictability (PP) is measured by the ratio between the signal and noise components. The signal, which is potentially predictable component, is related to atmospheric response to the boundary conditions such as SST. On the other hand, the noise is generated internally in the atmosphere and therefore a non-predictable part.

El Niño–Southern Oscillation is the largest natural modulator of interannual climate variability globally (Rasmusson and Wallace 1983; Glantz et al. 1991), which can influence the atmospheric predictability significantly. Several studies based on observational data during the last three decades documented the large-scale patterns of rainfall and temperature associated with ENSO. Ropelewski and Halpert (1987, 1989) highlighted wide regions in which precipitation anomalies revealed a noticeable response to the ENSO. Correlation based analyses also showed patterns of relatively strong relationships between ENSO and rainfall (e.g. Lau and Sheu 1988; Kiladis and Diaz 1989). The extent to which ENSO events influence the climate depends on the region, season, and also the strength and spatial distribution of the ENSO related SST anomalies. The changes of ENSO characteristics, predominantly its amplitude and frequency, have been the subject of recent research (An and Wang 2000; Chen et al. 2004). Observed records have shown that the ENSO SST variability has had large multidecadal changes during the twentieth century. For instance, ENSO had relatively strong amplitude during the period 1885–1910, proceeded by a few decades of relatively weak amplitude (1910–1965), and followed by a return to strong amplitude since about 1965 (Xue et al. 2003). Such changes in ENSO intensity may modulate the global climate circulation statistics and in turn may change the seasonal mean PP of atmospheric variables such as temperature and precipitation. This is because the predictable signal of atmospheric seasonal mean climate is considered to arise from the lower boundary conditions mainly related to SST anomalies in the ENSO region (Shukla et al. 2000).

Some studies have shown that atmospheric seasonal mean PP varies with time (Grimm et al. 2006; Kang et al. 2006). In these studies the time variation of PP is assessed by the relative sizes of the signal and noise components of the variability of particular atmospheric variables averaged over a season. The atmospheric PP depends on whether the signal is large enough to be seen above the noise. As such,

any information pertaining to changes in the magnitude of noise is also valuable for climate prediction. Any decrease in the noise or intensification in the signal implies an improvement in the seasonal mean PP. Many studies in the literature have characterized the SST-forced signal component and seasonal mean PP in ensembles of AGCM simulations. For example, Nakaegawa et al. (2004) found that the predictability of 500 hPa height in an AGCM for the boreal winter changed after 1950, mainly due to the increase in SST variability during that period. Wu and Kirtman (2006) explored the predictability of rainfall, surface pressure and 500 hPa height through the long-term integration of an interactive ensemble coupled GCM. They found that predictability, changes not only between the two phases of ENSO, i.e. El Niño and La Niña, but also from one season to another. Ferguson et al. (2011) examined interannual variability and trends in the SST-forced signal as well as the potential predictability of boreal winter precipitation anomalies through the 14 members of the National Aeronautics and Space Administration (NASA) Seasonal-to-Interannual Prediction Project (NSIPP-1) AGCM. They adduced that ENSO-related SST variability is the leading driver of the signal and potential predictability over the tropics, while over middle and high latitudes no significant association is reported between the principal modes of SST variability and predictability.

In all the studies described above and in many others found in the literature, the ensemble size and period of study is quite small to estimate the SST forced (signal) and chaotic internal variability (noise) components accurately; for instance, 3 members for the 34 years simulation in Sugi et al. (1997), 7 members for the 30 years simulation in Lang and Wang (2005), 10 members for the 50 years simulation in Nakaegawa et al. (2004), 4 members in Kang et al. (2006) and 14 members in Ferguson et al. (2011) for their twentieth century simulations. The technique of interactive ensemble coupling used by Wu and Kirtman (2006), actually reduces the impact of atmospheric internal dynamics, and underestimates the noise by about 10 % (Wu and Kirtman 2006). Typically the forced signal is estimated by an ensemble mean, but the ensemble sizes used in the above studies are too small to diminish the internal variability properly. The ensemble size needed to estimate the signal and S/N ratio depends upon the variable and the geographical region under consideration. For instance, the minimum ensemble size required to estimate precisely SST forced and free internal variability in the middle latitudes at 500 hPa height is about 20 (Déqué 1997), which is considerably larger than the ensemble sizes used in the predictability studies described above. Therefore, it is valuable to re-examine the quantitative measure of seasonal mean PP over the globe. One of the objectives of the present study is to address the aforementioned

shortcomings through utilizing a large ensemble size (100 members) and a longer period (139 years) in order to describe and assess the variations in the SST forced seasonal mean PP over the globe.

The main aim of this paper is to quantify whether the presumed changes in the ENSO characteristics, during the twentieth century, can induce changes in the amplitude of the seasonal mean signal and noise over the globe. These issues can be addressed in the context of ensemble AGCM climate simulations, forced with identical SST but starting with slightly different initial conditions. In this study, we have created a larger ensemble size to quantify more precisely the changes in the seasonal mean PP. The paper is organized as follows: Sect. 2 present a brief introduction to the model, experimentation and methodology. The twentieth century SST variability is analyzed in Sect. 3. The time variation of signal and noise variances of precipitation and 200 hPa height is presented in Sect. 4. In Sect. 5, we discussed the seasonal mean PP for precipitation, 200 hPa height and land surface temperature during the low and high SST variability periods. Section 6 provides a summary and conclusions.

## 2 Model, experiments and methods

An intermediate complexity model, the International Centre for Theoretical Physics AGCM (ICTPAGCM), also called Simplified Parameterizations, primitivE-Equation DYnamics (SPEEDY) is used in this study. The version of SPEEDY used here, has a standard horizontal resolution corresponding to a triangular spectral truncation to a total of 30 (T30) wavenumbers with  $96 \times 48$  Gaussian grids ( $3.75^\circ \times 3.75^\circ$ ) and 8 vertical layers. The dynamical core of the SPEEDY model is spectral, and it was developed at the Geophysical Fluid Dynamics Laboratory (Held and Suarez 1994). The parameterized processes include large-scale condensation, shallow and deep convection, short and long-wave radiation, surface fluxes of momentum, heat and moisture and vertical diffusion. For further details see Kucharski et al. (2013). The simplified physics in the SPEEDY model allow fast simulation of the climate without sacrificing scientific credibility to too great an extent. Indeed the SPEEDY model is comparatively a simple AGCM; it has been used in a number of studies dealing with a variety of aspects relating to tropical and extratropical climate variability. Some of the topics include: the impact of land-sea thermal contrast on extratropical planetary-scale variability (Molteni et al. 2011), the roles of external forcing and internal variability (King et al. 2010), the relationship between the Indian monsoon climate and the ENSO (Bracco et al. 2007; Yadav et al. 2010), and ENSO teleconnection studies (Herceg et al.

2011). The results presented in these and many other studies provide us confidence in the ability of our model to simulate the interdecadal variability of the atmospheric circulations as well as to estimate the response of the atmosphere to the ENSO related SST forcing, which is important for predictability studies.

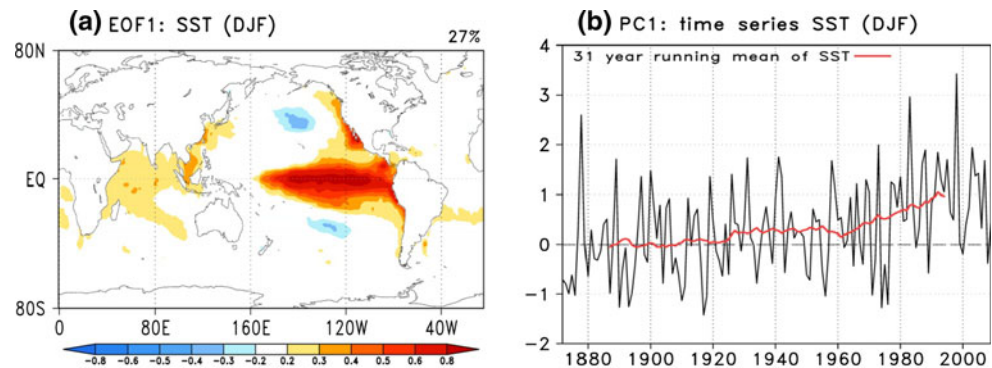
The experimentation is conducted by integrating the model over the period 1870–2009. The 100 member ensemble has been created by randomly perturbing the initial conditions, but keeping the SST boundary conditions identical. The Hadley Centre SST dataset HadISST1.1 is used for the model simulations (Rayner et al. 2003). The initial conditions of the model differ among ensemble members in the definition of tropical diabatic heating. Each member is initialized by adding slightly different tropical diabatic heating. The purpose behind using such a large ensemble size is to enhance the reliability and reduce the ambiguity of the simulations. With the help of this large ensemble of model integrations, the ability to detect the signal is enhanced since the noise, which is related to internal atmospheric variability, is reduced by the factor  $1/n$ , where  $n$  represents ensemble size (Rowell et al. 1995).

In order to remove the direct effects of the initial conditions, the first year of the ensemble integration is discarded as the model spin-up time. The analysis refers to the period 1871–2009, 139 years in total. We focus on observed SST, model simulated land surface temperature, precipitation and 200 hPa height. The latter is for the illustration of extratropical circulation anomalies associated with tropical forcing, particularly with ENSO. We consider the December–January–February (DJF) season over the globe, since this is the time during which the ENSO signal is the strongest (Wallace and Gutzler 1981; Yarnal and Diaz 1986). The model and observed seasonal mean anomalies for a given year are calculated by subtracting the model and observed overall seasonal mean respectively. However, for the case of 31 years moving window, the overall seasonal mean corresponds to those particular 31 years. For the assessment of seasonal mean PP, different measures can be found in the literature (Zwiers 1996; Rowell 1998). The signal-to-noise (S/N) ratio statistics is used to estimate the seasonal mean PP of precipitation and 200 hPa height and a “perfect model correlation” approach is used to assess the PP of land surface temperature. Student  $t$  test is used to check the significance of correlation and F-test is used to check the significance of the variance ratio.

## 3 Twentieth century SST variability

Figure 1a, b shows the leading empirical orthogonal function (EOF) eigenvector and associated principal component (PC) time series of the observed SST anomaly data

**Fig. 1** **a** The first EOF eigenvector of SST anomaly for DJF, with explained variance shown on *top right* of the panel. **b** The associated PC time series. The *red line* in **b** is the 31 years running mean of the PC time series. Unit is °C



over the globe for the DJF season. Figure 1a depicts the well-known global ENSO SST pattern. The leading spatial mode explains 27 % of the total SST anomaly variance, depicting positive values over much of the globe, with weak negative values over the North and South Pacific; the associated PC time series has strong interannual variability. To see the trends in the SST PC time series we use the moving-average method (Burroughs 1978). This is accomplished by “moving” the arithmetic mean values through the time series. The moving average is defined as the sum of  $N$  observations, divided by  $N$ , plotted at the central year in the observational series for every full  $N$  year window. The smoothed values cannot be calculated for the very first and last years in the data series. The red line shows (Fig. 1b) the 31 years moving average of the SST PC time series. In order to assess the statistical significance of the trend, we use non-parametric rank-based statistical test (Mann 1945; Kendall 1975) namely Mann–Kendall (MK). MK test has been extensively used with environmental and hydro-meteorological time series (e.g. Hipel and McLeod 1994; Zhang et al. 2000). The SST PC time series is found to have a statistically significant increasing trend ( $p$  value  $< 0.05$ ). Considering Fig. 1b we define two periods, 1920–1950 and 1970–2000 which have low and high variability respectively. The standard deviations (SDs) for these two periods are 0.71 and 1.15 °C, respectively, with a percentage change of 62 %, over the Niño-3.4 region (Trenberth 1997). Two thousand Monte Carlo (MC) trials are carried out to check the difference in the SDs between the two periods. The two SDs appear statistically significantly different by using MC at our significance threshold of  $\alpha = 0.05$ . Besides this, if we remove the trend first and calculate the SDs again, the values are 0.69 and 1.07, for the periods of low and high SST variability, respectively, with a percentage change of 55 %, but still statistically significantly different by using MC.

Now we calculate the pattern of change to SST variations for the twentieth century by computing the SST variance on a 31 years moving window. The moving variance method is described in Kang et al. (2006)

and is similar to the moving average method above, but with two differences. Firstly, the variance is calculated on each 31 year sample instead of mean. Secondly, the moving variance calculation is applied to the SST data at each grid-point of the SST field. Once the moving variance of the SST field has been calculated, the overall mean of the spatial time series is removed at each grid point, and the fields are multiplied by an area-weighting factor (square root of the cosine of latitude). Finally an EOF analysis is carried out. The leading EOF eigenvector is characterized by positive values over the globe, and explains 56 % of the total variance (Fig. 2a). The associated PC time series, indicate statistically significant ( $p$  value  $< 0.05$ ) increasing trend in the amplitude of the SST variations after 1920s (Fig. 2b). The increase in the amplitude of SST variability is quite prominent, particularly over the ENSO region. The decreasing behavior until 1920s and rising to positive values toward the end of the record (Wang and Ropelewski 1995). The reason for choosing the 31 years window, to calculate the moving average and variance is to have an assessment on the time variation of seasonal mean potential predictability in the context of climate change (WMO 2007). Besides 31 years window, we also checked the sensitivity of our results (positive trend) to different window length (results not shown). We found that the spatial pattern remains almost unchanged, however, PC time series, is sensitive (fewer data points lead to more fluctuations) to the choice of the window length, but still it shows overall increasing trend.

Previous works described that the strong SST anomalies associated with an ENSO event may continue from seasons-to-years and have strong influence on the climate on a variety of spatial scales ranging from regional to global (Quan et al. 2006). Xue et al. (2003) elucidated that change in the amplitude of SST variability, particularly in the ENSO region, causes the changes in seasonal mean PP across the globe. In this paper we use ensemble of model simulations with longer integration period to quantify these changes.

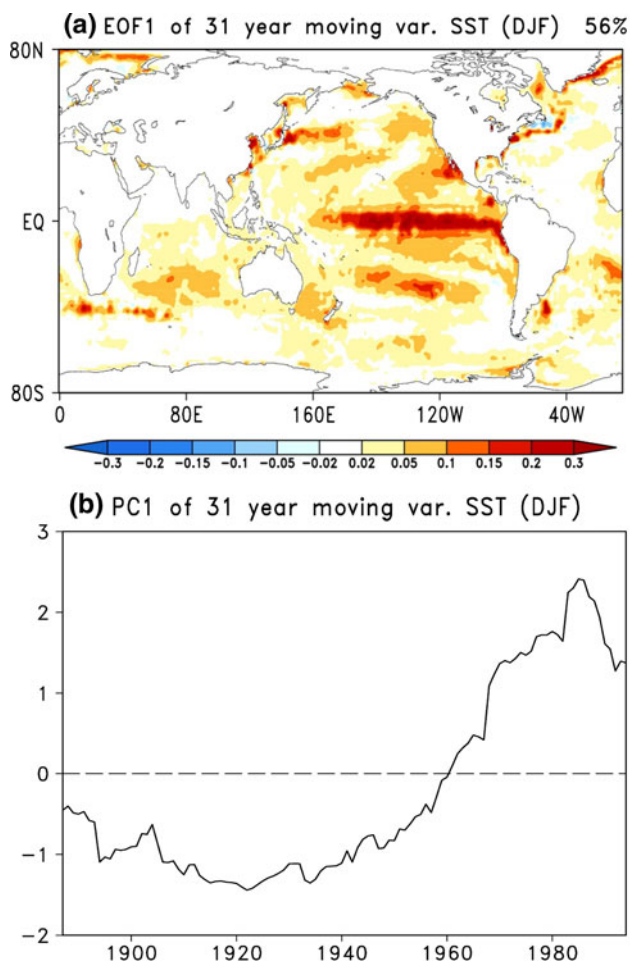


**Fig. 2** **a** The first EOF eigenvector for DJF, with explained variance shown on *top right* of the panel. **b** The associated PC time series of the 31 years moving variance of SST over the globe. The unit is  $^{\circ}\text{C}^2$

#### 4 Time variation of signal and noise

Now we examine how the signal and noise variances of the seasonal mean precipitation have changed with time for the twentieth century by using EOF analysis. The signal component is calculated from the ensemble mean variance, and the noise component, is quantified by the ensemble spread resulting from different atmospheric initial conditions based on a 31 years moving window. The method of creating variance data and use of EOF analysis to the signal and noise components of seasonal mean precipitation is similar to that of SST (see Sect. 3). The leading EOF of the 31 years moving signal and noise variances, explain about 68 and 37 % of the total variance of each individual variable respectively (Fig. 3a, b). The PC time series of moving signal variance of precipitation (Fig. 3c) show similar trend ( $p$  value  $<0.05$ ) to that of SST variance (Fig. 2b), with more or less same fluctuations during the whole period. For instance, a sharper increase from 1970s until 1990s. Correlation between the

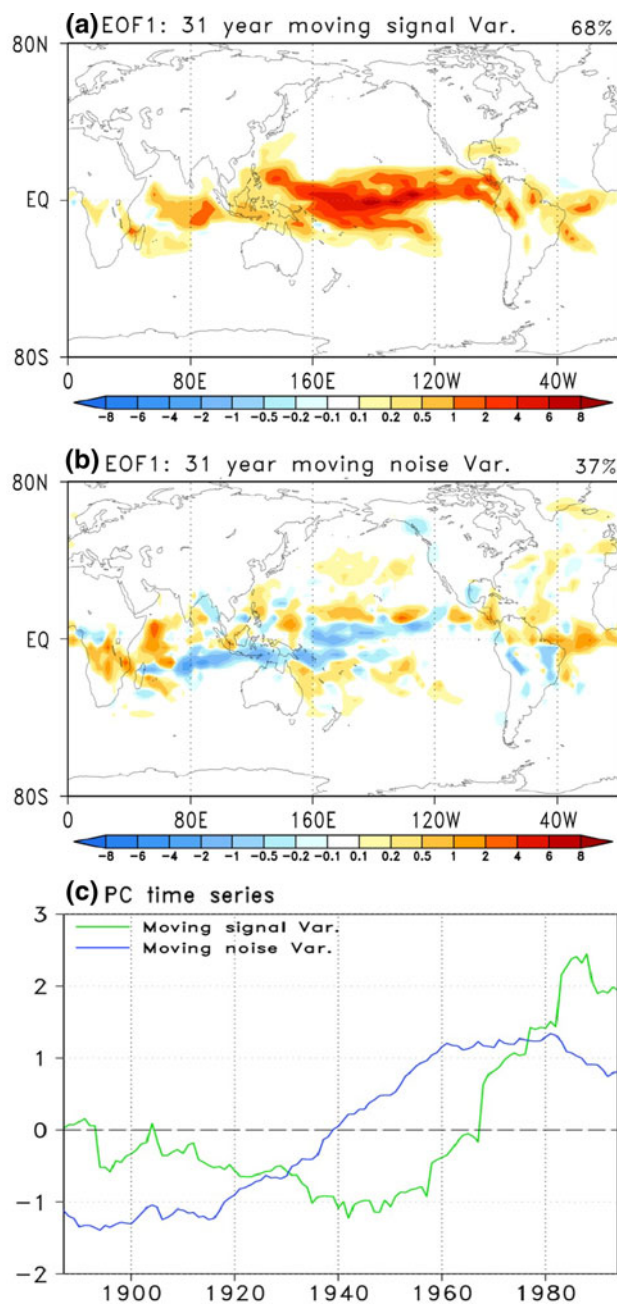


**Fig. 3** The first EOF eigenvector, of model-simulated DJF precipitation with explained variance shown on *top right* of the panel. **a** The signal variance, **b** the noise variance, and **c** the associated time series. In **c**, *green* and *blue solid lines* represent the time series of PC for 31 years moving signal, noise variances respectively. The unit is  $\text{mm}^2 \text{day}^{-2}$  for signal and noise

PC time series of SST variance and precipitation signal is 0.92. On the other hand the noise PC time series increases more steadily and has correlation 0.76 with leading PC of SST variance. From the spatial map (Fig. 3a), the signal variance of precipitation is pronouncedly increased over the Equatorial Pacific (EP) and Indian oceans, as well as

land regions associated with ENSO teleconnections, for example northern south America, and the Maritime continent. This suggests that strong SST anomalies in the ENSO region are associated with a greater precipitation signal over these regions (Halpert and Ropelewski 1992). On the other hand, the change in variability of noise variance (Fig. 3b) is more or less randomly distributed, and even has a negative sign in many of the tropical regions. This means that the increased ENSO SST variability has a quite complicated (some areas have negative and some have positive values), influence on the noise as well. In general the analysis results presented here agree with the previous studies discussing the seasonal mean PP of DJF precipitation (Kang et al. 2006; Ferguson et al. 2011), with some regional differences which may be attributed to the fact that signal and noise variability is essentially model dependent (Kang and Shukla 2006).

For the time variation of signal and noise variances of 200 hPa height, we focus on the PNA region. Similar, to the precipitation analysis, the leading EOF of the 31 years moving signal and noise variances, explain about 64 and 56 % of the total variance of each individual variable respectively (Fig. 4a, b). The leading PC time series of signal and noise of 200 hPa height (Fig. 4c) is quite similar to leading PCs of SST and signal, noise of precipitation (Figs. 2b, 3c). Correlation between the PCs of moving variance of SST and 200 hPa height signal is 0.91. From the spatial map (Fig. 4a) the signal variance of 200 hPa height is increased over the PNA region due to the strong teleconnection between SST anomalies in the ENSO region and PNA circulation anomalies. On the other hand, the change in variability of noise variance (Fig. 4b) is quite high over most of the PNA region but it also has a negative sign in some parts of PNA, due to the same fact that the ENSO SST variability has regionally quite complicated influence on the noise.

In this analysis we have only considered the leading EOF to describe the time variation of SST variability, as well as the signal and noise of precipitation and 200 hPa height. This is for the two reasons. Firstly, the second and third modes explain only 13–20 and 2–7 % of total variance, respectively for all variables presented above. This indicates that in this case, the time variations of signal and noise can be represented rather assertively by a single global pattern. Secondly the other EOFs do not appear to be related to changes in the characteristics of ENSO. As the focus of the current study is the variation of PP in response to these changes in ENSO, we consider only the first EOF. In the next section we discuss the quantitative assessment of signal, noise and PP based on two periods (low and high SST variability) of the twentieth century, which we believe to be under two different regimes of ENSO variability.

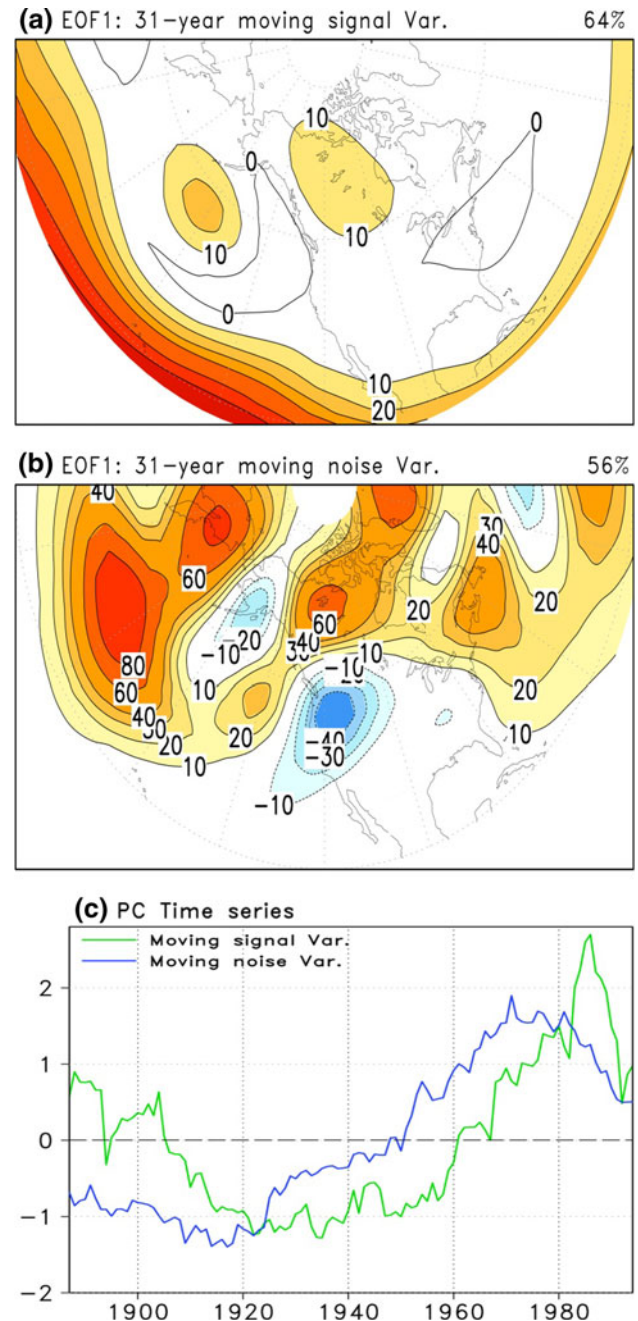


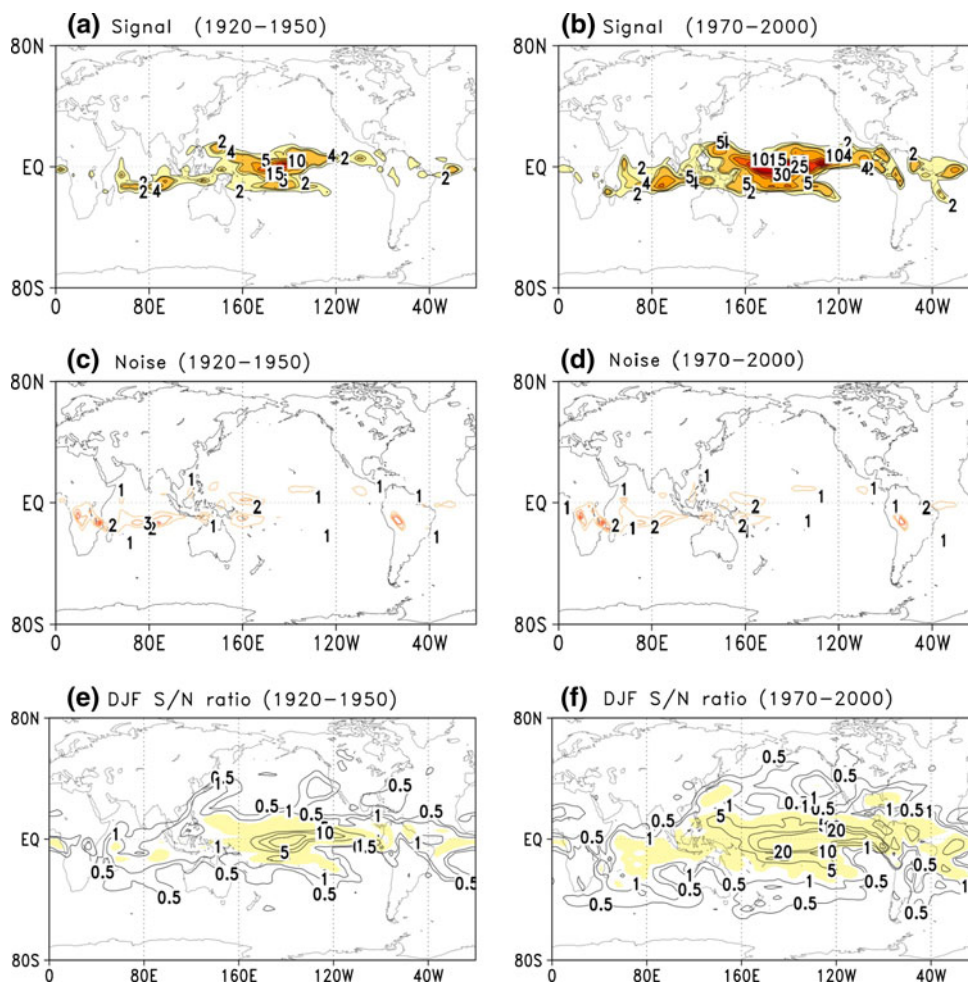
**Fig. 4** The first EOF eigenvector, of model-simulated DJF 200 hPa height with explained variance shown on *top right* of the panel. **a** The signal variance, **b** the noise variance, and **c** the associated time series. In **c**, *green* and *blue solid lines* represent the time series of PC for 31 years moving signal, noise variances respectively. The unit is  $10 \text{ m}^2$  for signal and noise

## 5 Quantitative assessment of potential predictability

### 5.1 Precipitation

Figure 5e, f shows the S/N ratios for DJF precipitation for the low and high SST variability periods with areas where

**Fig. 5** Variance of the seasonal mean DJF precipitation for the low and high variability periods; **a, b** for signal, **c, d** for noise and **e, f** for the S/N ratio. The unit is  $\text{mm}^2 \text{day}^{-2}$  for signal and noise. **e, f**, the shaded areas indicate the region where the ratio is statistically significant at the 5 % level



the S/N is significantly greater than 1 colored. Also shown in Fig. 5a–d are the signal and noise respectively, to identify the relative contribution of each component in the change of S/N ratio. During the high SST variability period, the signal has relatively larger values, compared with the signal variance of the low variability period (Fig. 5a, b). The noise variance shows lower values during the high SST variability period over tropical areas in comparison to low SST variability period. The S/N ratio varies globally (Fig. 5e, f): it is generally higher at low latitudes, with a maximum value over the equatorial regions, and gradually decreases toward high latitudes.

The quantitative comparison of the signal and noise for DJF precipitation during the low and high SST variability periods is also presented here. There have been several studies which illustrate potential relationships among the different phases of the ENSO and interannual climatic variability over wide regions of the world. These include global-scale (Ropelewski and Halpert 1987; Kiladis and Diaz 1989) to regional-scale studies both in the tropics (Rogers 1988; Goswami 2004; Kumar et al. 2007) and extratropics (Yarnal and Diaz 1986). For the quantitative

comparison the values are computed over the wider domains ( $10^{\circ}\text{S}$ – $30^{\circ}\text{N}$ ,  $140^{\circ}\text{E}$ – $240^{\circ}\text{E}$ ) of EP and South Asia (SA) ( $10^{\circ}\text{S}$ – $30^{\circ}\text{N}$ ,  $60^{\circ}\text{E}$ – $120^{\circ}\text{E}$ ). The quantitative analysis, over the EP, shows that the signal variance is 4.73 and  $8.89 \text{ mm}^2 \text{day}^{-2}$ , indicating an increase in the SST-forced response by 87 %, while the noise variance is 3.17 and  $2.83 \text{ mm}^2 \text{day}^{-2}$ , which indicates a decrease in the internal variability by 10 %, for the low and high SST variability periods respectively (both statistically significantly different using MC). Similarly, over SA, the signal variance is 0.9 and  $1.4 \text{ mm}^2 \text{day}^{-2}$ , indicating an increase in the SST-forced response by 56 % (statistically significantly different using MC), while the noise variance is 2.51 and  $2.50 \text{ mm}^2 \text{day}^{-2}$ , which indicates no considerable change in the internal variability.

Figure 6 exhibits the ratio of S/N ratios for DJF precipitation between the low and high SST variability periods, which is important to highlight the changes in the seasonal mean PP between the two periods. A value of “1” indicates that there is no difference between the S/N ratios for the two periods. From the Fig. 6 we observe that the S/N ratio is relatively increased over the equatorial tropical

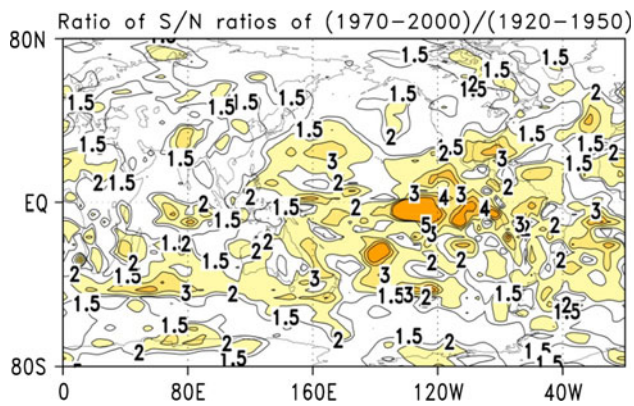


**Fig. 6** Ratio of the S/N ratios for DJF precipitation during the low and high variability periods

Pacific, particularly over the eastern EP during the high SST variability period. Over the land, the increase is prominent over South America, southeast United States, some parts of Canada, the Sahel region and the North-western regions of India (including northern Pakistan). Yadav et al. (2010) examined the influence of ENSO on the interannual variability of the Northwest India winter precipitation (NWIWP) by using the station data of Indian Meteorological Department and reanalysis data from 1950 to 2008, resulting from SSTs. From the observational data they found that the interannual variability of NWIWP was influenced by ENSO during recent decades. The analysis of signal and S/N ratio for DJF precipitation estimated in this study agrees with results in Yadav et al. (2010), particularly in terms of the increase in the SST-forced response (signal) and hence S/N ratio.

## 5.2 Geopotential height

The geographical distribution of S/N ratio is shown in Fig. 7e, f for 200 hPa height during the low and high SST variability periods. Also shown in Fig. 7a–d are the signal and noise respectively, to identify the relative contribution of each variable to any change in the S/N ratio. During the high SST variability period, signal has relatively large values, compared with the signal variance of the low variability period (Fig. 7a, b). The values for the noise variance for the two periods are quite similar, with slightly higher values during the high SST variability period. The S/N ratio is usually higher in low latitudes; with a maximum value over the equatorial regions, decreasing toward high latitudes (Fig. 7e, f). The signal variance is averaged over the extratropical region ( $25^{\circ}$ – $70^{\circ}$ N,  $60^{\circ}$ W– $180^{\circ}$ ) for the low and high variability periods, which are 385 and 504  $\text{m}^2$  respectively indicating an increase in the SST-forced response by 30 % (statistically significantly different using MC). Similarly, the averaged noise variance over

the region is 1,840 and 2,193  $\text{m}^2$  for the two periods, indicating an increase in the internal variability (noise) by 19 % (statistically significantly different using MC). This shows that the predictability change for 200 hPa height is largely attributable to the signal change during the two periods. The ratio of S/N ratios during the low and high SST variability periods is also calculated and it is shown in Fig. 8. As expected from the foregoing analysis, the ratio is greater than unity over the extratropical region and over the PNA region, which indicates that the S/N ratio has increased during the high SST variability period.

Many studies in literature have estimated the S/N ratio over the extratropics for boreal winter (Sugi et al. 1997; Lang and Wang 2005; Nakaegawa et al. 2004; Kang et al. 2010). Very recently, Kang et al. (2010) estimated the S/N ratio of the 200 hPa geopotential height. They used the hindcast data of seven European ocean–atmosphere coupled models under “Development of a European multi-model ensemble system for seasonal to interannual prediction (DEMETER)” project for the 22 years, from 1980 to 2001. They found that the S/N ratio is less than unity everywhere over the extratropics with maximum values of about 0.7 in the PNA region during the boreal winter. The analysis of 200 hPa height over the extratropics estimated by using an intermediate complexity model, SPEEDY, matches well with results in Kang et al. (2010), and shows good PP skill over extratropical regions (including PNA).

The time variation described in Sect. 4 and the quantitative assessment of signal and noise over the PNA region reveals that the signal increased, but the noise also increased, during the high SST variability period. This might be because the ENSO related SST anomalies stimulate the extratropical circulation anomalies directly through the teleconnection mechanism (Hoskins and Karoly 1981) and indirectly by affecting the non-linear atmospheric processes related with the synoptic transient (Ting and Held 1990). The transient statistics are strongly affected by ENSO (Lau and Nath 1991) and that the transient anomalies play an important role in the extratropical circulation anomalies, particularly over the PNA region (Pan et al. 2006). The transient anomalies also contribute to a certain portion of seasonal mean circulation anomalies in the PNA region and provide a big fraction of the predictive signal in that region. Therefore, the prediction skill of seasonal mean anomalies in the PNA region is affected not only by the ENSO SST anomalies but also due to the extratropical transient.

Now, we analyze whether there is any change (increase/decrease) in the signal or noise component of synoptic transient during the low and high SST variability periods. The transient activity is estimated by the root-mean-square (RMS) of the high-frequency component of 200 hPa height



**Fig. 7** Variance of the seasonal mean DJF 200 hPa height for the low and high variability periods; **a, b** for signal, **c, d** for noise and **e, f** for the S/N ratio. The contour interval is  $5 \times 10^2 \text{ m}^2$  for signal and  $10 \times 10^2 \text{ m}^2$  for noise. **e, f**, the shaded areas indicate the region where the ratio is statistically significant at the 5 % level

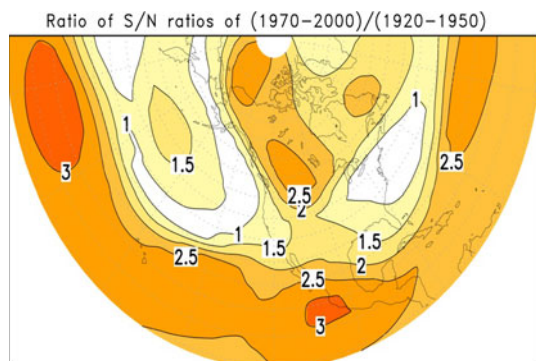
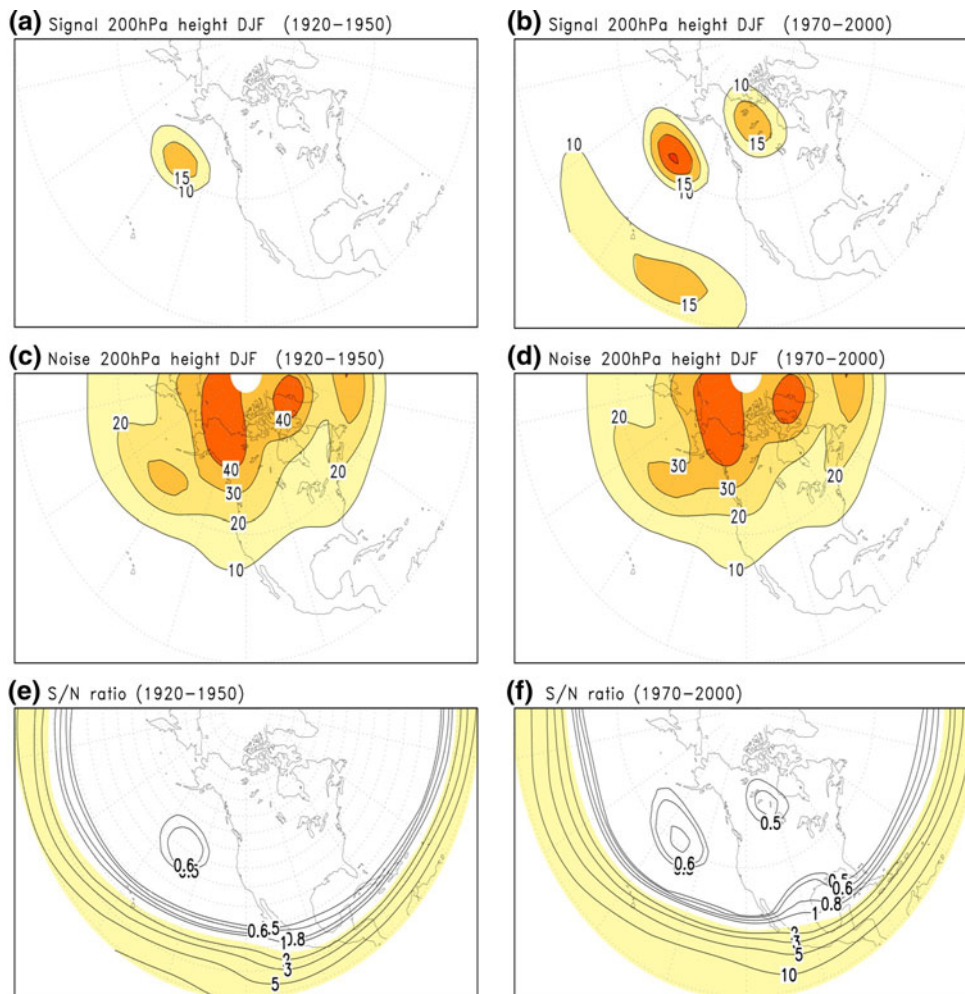


**Fig. 8** Ratio of the S/N ratios for DJF 200 hPa height during the low and high variability periods

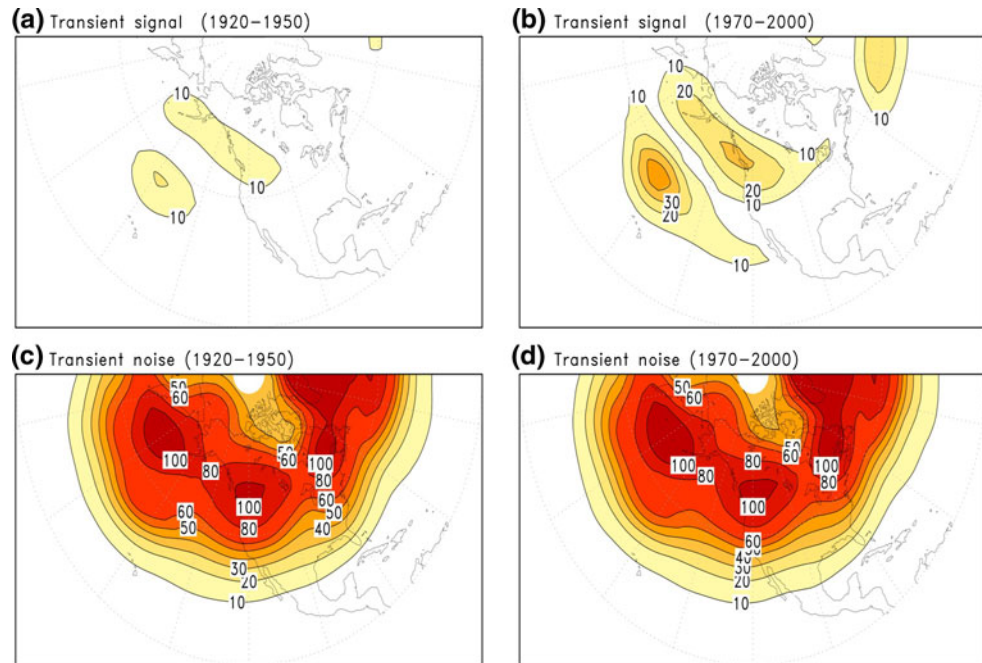
with a time scale of 2–10 days. Figure 9 shows signal and noise variance computed for the transient. The signal variance of the transient during the high SST variability period shows relatively large values (Fig. 9a, b). As the synoptic transient also produces unpredictable noise in the prediction. Figure 9c, d shows the noise variance of transient during the low and high SST variability periods.

Interestingly the noise variance of transient also remains more or less constant (slight increase) like the 200 hPa noise variance during the low and high SST variability periods. The signal and noise variance of transient is averaged over the PNA region for the low and high SST variability periods. For signal, the values are 6.6 and  $10 \text{ m}^2$ , indicating an increase in the SST-forced response by 50 % and for the noise, the values are 55.1 and  $62.1 \text{ m}^2$ , which indicates an increase in the noise by 12 % (both statistically significantly different using MC). The quantitative analysis shows that the signal component is increased more than the noise component. This enhancement in the signal component could also provide a positive feedback to the 200 hPa height predictability.

### 5.3 Land surface temperature

Finally we show the seasonal mean PP for DJF land surface temperature, measured here in terms of the perfect model correlation, during the low and high SST variability periods. The correlation skill of the perfect model is estimated by considering one of the ensemble simulations as

**Fig. 9** Variance of the transient activity for the low and high SST variability periods; **a, b** for signal and **c, d** for noise. The unit is  $m^2$  for signal and noise



observation, and the member (observation) is correlated with the ensemble-mean of the rest of ensemble members. Following to the number of ensembles, 100 correlations are averaged for this case. The raw correlation coefficients (CC) cannot be added directly, so they are first transformed into a new variable called the Fisher Z value (Faller 1981). Figure 10a–c shows the statistically significant PP for the low and high SST variability periods as well as the percentage difference between the two periods. A comparison between Fig. 10a, b clearly indicates that during the low(high) SST variability, the correlation skill is also low(high). In general, we observe an increase in the correlation skill ( $CC > 0.7$ ) over the equatorial regions of Africa, South America and Indonesia (including adjacent archipelago regions). In the other areas, we see the moderate increase ( $CC > 0.2$ ) in the skill, including Australia, North America and over Canada and Alaska. The higher correlation skill over North America, Canada and Alaska during DJF, shows the strong impact of SST on these regions (Halpert and Ropelewski 1992; Ropelewski and Halpert 1986).

Earlier predictability studies conducted using models have found higher values for the PP of surface air temperature over the oceans and low PP over land for different seasons (Sugi et al. 1997; Lang and Wang 2005; Boer and Lambert 2008). For instance, Lang and Wang (2005) studied the PP of surface air temperature for different seasons by using 7 members of (IAP9L-AGCM). Their results showed high PP values over the oceans and low ones over land. Similarly, Boer and Lambert (2008) also estimated high PP of temperature over ocean and weak over land areas by using 21 state-of-the-art coupled climate

models. In this study 100 members are used to estimate the land surface temperature predictability. The large members and longer period enable us to estimate both higher as well as precise PP over wide regions of the globe, which is lacking in the similar model based studies described above (few members and small data length).

## 6 Summary and conclusions

The changes in the seasonal mean PP for DJF precipitation, 200 hPa height and land surface temperature are investigated over the globe using an ensemble containing 100 members (conducted with SPEEDY model) from 1871 to 2009. Each ensemble member is forced by the same observed SST but differs only slightly in their initial conditions. The results presented here are based on the identification of two periods of observed SST data, which we describe as the low (1920–1950) and the high (1970–2000) SST variability periods. The standard deviation values averaged for the Niño-3.4 region, for these periods of low and high SST variability are 0.71 and 1.15  $^{\circ}C$ , which give a percentage change of 62 % for the DJF season. The leading EOF eigenvector and the associated PC time series, indicate that the amplitude of SST variations have positive trend since 1920s (to recent years), particularly over the ENSO SST region. Previous studies have recognized that the changes in tropical SST (linked with ENSO) strongly interact with both the tropical and extratropical atmosphere. Understanding the patterns of variability within SST itself is important for seasonal mean predictability, where SST forcing is the primary source of predictability.

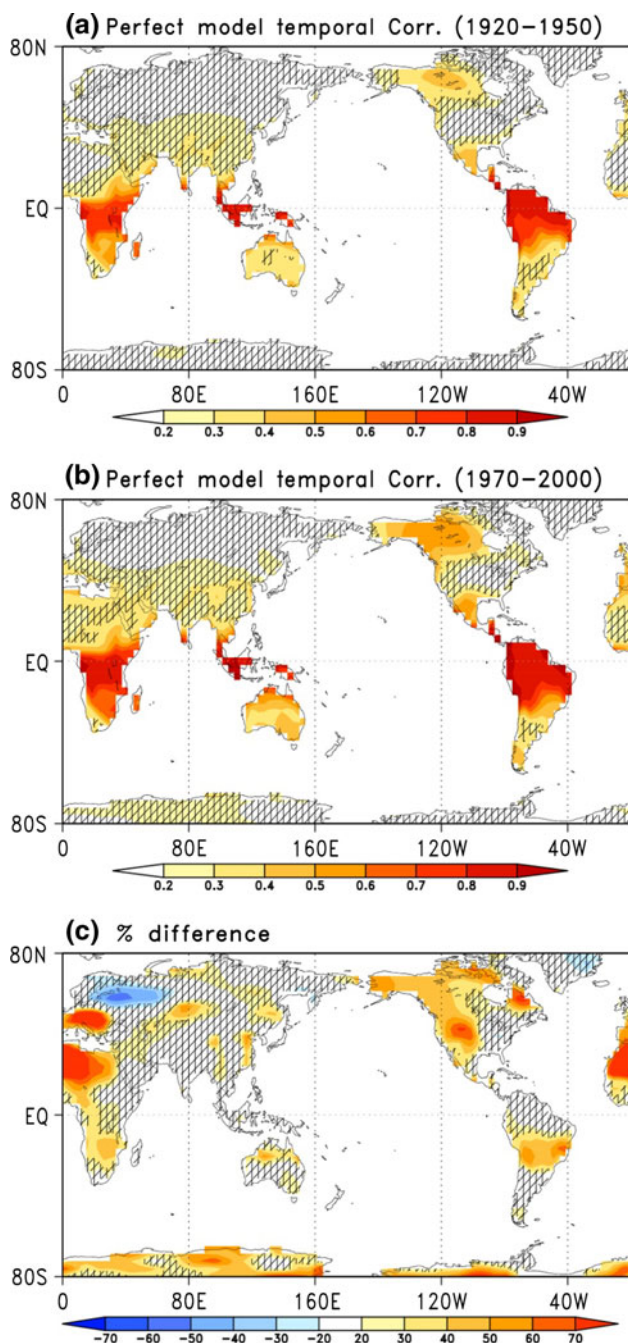


**Fig. 10** Perfect model correlation of model-simulated DJF land surface temperature for **a** low SST variability during 1920–1950, **b** high SST variability during 1970–2000, and **c** the % difference. Values are hatched where the correlation is not statistically significant at the 5 % level

Signal (SST-forced) and noise (free variability) variances and the S/N ratio for the seasonal mean precipitation and 200 hPa height indicate that the seasonal mean PP has increased during the twentieth century, and that in particular this increase is large during the period 1970–2000. This is because the SST-forced component, i.e. the signal

part has increased during this period. We also investigate the signal variance, computed for the seasonal mean transient during the low and high SST variability periods, which shows relatively high value of signal variance during the high SST variability period. Since the synoptic transient also produces unpredictable noise in the prediction, the noise variance of transient during the low and high SST variability periods remains more or less constant (slight increase). The grid point values for the signal and noise variance of transient activity, over the PNA region for the low and high SST variability periods indicates an increase in the SST-forced response by 50 %, while the noise increases only 12 %. This indicates that the transient signal component is increased more than the noise component and could provide a positive feedback to the 200 hPa height predictability. The perfect model correlations for seasonal mean land surface temperature show clearly the seasonal mean PP increased during the twentieth century. Comparing the PP results presented in this study with other studies using the models, shows the potential advantage of using such a large ensemble size with a longer period of integration. The large ensemble size makes possible to estimate SST forced (signal) and internal (noise) variability more accurately (Branković and Palmer 1997) than would be possible using a smaller ensemble.

In this study, only SST is used as an external boundary condition; however, the effects of, for example, sea ice, soil moisture, snow cover, and other land surface properties are also important in deriving accurate estimation for PP (Fennessey and Shukla 1999; Douville et al. 2001). Therefore, the quantitative assessment of PP presented here is exclusively related to SST and should be seen as the lower limit of seasonal mean PP of the model, reflecting the underlying assumptions of perfect model. It is not stringently a measure for true predictability (assessment against observation). Also in the present study, we do not consider the likely influence of incorrectly recorded SST data over time, particularly before 1950 (Goddard and Mason 2002), because our principal focus is on the change in seasonal mean PP under given history of SST.

Recently, it has been documented that human-induced global warming may have an influence on the frequency and amplitude of ENSO (Fedorov and Philander 2000; Collins et al. 2010). The present findings suggest that the seasonal mean PP increased with time over the twentieth century because the SST-forced signal increased. If ENSO variance continues to increase, the predictability of seasonal mean climate may also increase in the future.

**Acknowledgments** The authors thank the two anonymous reviewers for their constructive suggestions that improved the paper significantly. The authors would like to acknowledge the Center of Excellence for Climate Change Research (CECCR), Department of Meteorology and Deanship of Graduate Studies, King Abdulaziz

University (KAU), Jeddah Saudi Arabia for providing the necessary computational resources and support to carry out this study. The Earth System Physics group of ICTP, Trieste, Italy is acknowledged for providing the SPEEDY model.

## References

- An SI, Wang B (2000) Interdecadal change of the structure of the ENSO mode and its impact on the ENSO frequency. *J Clim* 13:2044–2055
- Boer GJ, Lambert SJ (2008) Multi-model decadal potential predictability of precipitation and temperature. *Geophys Res Lett* 35:L05706. doi:10.1029/2008GL033234
- Bracco A, Kucharski F, Molteni F, Hazeleger W, Severijns C (2007) A recipe for simulating the interannual variability of the Asian summer monsoon and its relation with ENSO. *Clim Dyn* 28:441–460
- Branković C, Palmer TN (1997) Atmospheric seasonal predictability and estimates of ensemble size. *Mon Weather Rev* 125:859–874
- Burroughs WJ (1978) On running means and meteorological cycles. *Weather* 33:101–109
- Chen D, Cane MA, Kaplan A, Zebiak SE, Huang DJ (2004) Predictability of El Niño over the past 148 years. *Nature* 428:733–736
- Collins M et al (2010) The impact of global warming on the tropical Pacific Ocean and El Niño. *Nature* 3:391–397
- Déqué M (1997) Ensemble size for numerical seasonal forecasts. *Tellus* 49A:74–86
- Douville H, Chauvin F, Broqua H (2001) Influence of soil moisture on the Asian and African Monsoons. Part I: mean monsoon and daily precipitation. *J Clim* 14:2381–2403
- Faller AJ (1981) An average correlation coefficient. *J Appl Meteorol* 20:203–205
- Fedorov AV, Philander SG (2000) Is El Niño changing? *Science* 288:1997–2002
- Fennessy MJ, Shukla J (1999) Impact of initial soil wetness on seasonal atmospheric prediction. *J Clim* 12:3167–3180
- Ferguson IM, Duffy PB, Philip TJ, Liang X (2011) Non-stationarity of the signal and noise characteristics of seasonal precipitation anomalies. *Clim Dyn* 36:739–752
- Glantz MH, Katz RW, Nicholls N (1991) *Teleconnections linking worldwide climate anomalies*. Cambridge University Press, New York, p 535
- Goddard L, Mason SJ (2002) Sensitivity of seasonal climate forecasts to persisted SST anomalies. *Clim Dyn* 19:619–632
- Goswami BN (2004) Interdecadal change in potential predictability of the Indian summer monsoon. *Geophys Res Lett* 31:L16208
- Grimm AM, Sahai AK, Ropelewski CF (2006) Interdecadal variations in AGCM simulation skills. *J Clim* 19:3406–3419
- Halpert MS, Ropelewski CF (1992) Surface temperature patterns associated with the Southern Oscillation. *J Clim* 5:577–593
- Held IM, Suarez MJ (1994) A proposal for the intercomparison of the dynamical cores of atmospheric general circulation models. *Bull Am Meteorol Soc* 75:1825–1830
- Herceg I, Branković Č, Kucharski F (2011) Winter ENSO teleconnections in a warmer climate. *Clim Dyn* 38:1593–1613
- Hipel KW, McLeod AI (1994) *Time series modelling of water resources and environmental systems*. development in water science, vol. 45. Elsevier, Amsterdam
- Hoskins B, Karoly D (1981) The steady linear response of a spherical atmosphere to thermal and orographic forcing. *J Atmos Sci* 38:1179–1196
- Kang IS, Shukla J (2006) Dynamic seasonal prediction and predictability of the monsoon. *The Asian monsoon*. Springer, Chichester
- Kang IS, Jin EK, An KH (2006) Secular increase of seasonal predictability for the 20th century. *Geophys Res Lett* 33:L02703
- Kang IS, Kug JS, Lim MJ, Choi DH (2010) Impact of transient eddies on extratropical seasonal mean predictability in DEMETER models. *Clim Dyn* 37:509–519
- Kendall MG (1975) *Rank correlation methods*. Griffin, London
- Kiladis GN, Diaz HF (1989) Global climatic anomalies associated with extremes in the southern oscillation. *J Clim* 2:1069–1090
- King MP, Kucharski F, Molteni F (2010) The roles of external forcings and internal variabilities in the northern hemisphere atmospheric circulation change from the 1960s to the 1990s. *J Clim* 23:6200–6220
- Kucharski F, Molteni F, King MP, Farneti R, Kang IS (2013) On the need of intermediate complexity general circulation models. *Bull Am Meteor Soc* 94:25–30
- Kumar P, Rupa Kumar K, Rajeevan M, Sahai AK (2007) On the recent strengthening of the relationship between ENSO and northeast monsoon rainfall over South Asia. *Clim Dyn* 28:649–660
- Lang X, Wang H (2005) Seasonal differences of model predictability and the impact of SST in the Pacific. *Adv Atmos Sci* 22:103–113
- Lau N, Nath M (1991) Variability of the baroclinic and barotropic transient eddy forcing associated with monthly changes in the midlatitude storm tracks. *J Atmos Sci* 48:2589–2613
- Lau KM, Sheu PJ (1988) Annual cycle, quasi-biennial oscillation, and southern oscillation in global precipitation. *J Geophys Res* 93:10975–10988
- Mann HB (1945) Nonparametric tests against trend. *Econometrica* 13:245–259
- Molteni F, King MP, Kucharski F, Straus DM (2011) Planetary-scale variability in the northern winter and the impact of land-sea thermal contrast. *Clim Dyn* 37:151–170
- Nakaegawa T, Kanamitsu M, Smith TM (2004) Interdecadal trend of precipitation skill in an ensemble of AMIP-type experiment. *J Clim* 17:2881–2889
- Pan L, Jin F, Watanabe M (2006) Dynamics of synoptic eddy and low-frequency flow interaction. Part III: baroclinic model results. *J At Sci* 63:1709–1725
- Quan X, Hoerling M, Whitaker J, Bates G, Xu T (2006) Diagnosing sources of US seasonal forecast skill. *J Clim* 19:3279–3293
- Rasmusson EM, Wallace JM (1983) Meteorological aspects of the El Niño/Southern Oscillation. *Science* 222:1195–1202
- Rayner NA, Parker DE, Horton EB, Folland CK, Alexander LV, Rowell DP, Kent EC, Kaplan A (2003) Global analyses of SST, sea ice, and night marine air temperature since the late nineteenth century. *J Geophys Res* 108:(D14). doi:10.1029/2002JD002670
- Rogers JC (1988) Precipitation variability over the Caribbean and tropical Americas associated with the southern oscillation. *J Clim* 1:172–182
- Ropelewski CF, Halpert MS (1986) North American precipitation and temperature patterns associated with the El Niño-Southern Oscillation (ENSO). *Mon Wea Rev* 114:2352–2362
- Ropelewski CF, Halpert MS (1987) Global and regional scale precipitation patterns associated with the El Niño/Southern Oscillation. *Mon Wea Rev* 115:1606–1626
- Ropelewski CF, Halpert MS (1989) Precipitation patterns associated with the high index phase of the southern oscillation. *J Clim* 2:594–614
- Rowell DP (1998) Assessing the potential seasonal predictability with an ensemble of multidecadal GCM simulations. *J Clim* 11:109–120
- Rowell DP, Folland CK, Maskell K, Ward MN (1995) Variability of summer rainfall over tropical North Africa (1906–92): observations and modeling. *Quart J Roy Meteor Soc* 121:699–704
- Shukla J et al (2000) Dynamical seasonal prediction. *Bull Am Meteor Soc* 81:2593–2606
- Sugi M, Kawamura R, Sato N (1997) A study of SST-forced variability and potential predictability of seasonal mean fields using the JMA global model. *J Meteorol Soc Jpn* 75:717–736

- Ting M, Held I (1990) The stationary wave response to a tropical SST anomaly in an idealized GCM. *J Atmos Sci* 47:2546–2566
- Trenberth K (1997) The definition of El Niño. *Bull Am Meteor Soc* 8:2771–2777
- Wallace J, Gutzler D (1981) Teleconnections in the geopotential height field during the Northern Hemisphere winter. *Mon Weather Rev* 109:784–812
- Wang XL, Ropelewski CF (1995) An assessment of ENSO-scale secular variability. *J Clim* 8:1584–1599
- World Meteorological Organization (2007) The role of climatological normals in a changing climate. WCDMP 61, WMO/TD-1377, p 43
- Wu RG, Kirtman BP (2006) Changes in spread and predictability associated with ENSO in an ensemble of coupled GCM simulations. *J Clim* 19:4378–4396
- Xue Y, Smith TM, Reynolds RW (2003) Interdecadal changes of 30-yr SST normals during 1871–2000. *J Clim* 16:1601–1612
- Yadav RK, Yoo JH, Kucharski F, Abid MA (2010) Why Is ENSO influencing Northwest India Winter precipitation in recent decades? *J Clim* 23:1979–1993
- Yarnal B, Diaz HF (1986) Relationships between extremes of the southern oscillation and the winter climate of the Anglo–American Pacific coast. *J Climatol* 6:197–219
- Zhang X, Vincent LA, Hogg WD, Niitsoo A (2000) Temperature and precipitation trends in Canada during the 20th century. *Atmos Ocean* 38:395–429
- Zwiers FW (1996) Interannual variability and predictability in an ensemble of AMIP climate simulations conducted with the CCC GCM2. *Clim Dyn* 12:825–848